Carbon, Helium and Proton Kinetic Temperatures in a Cygnus Loop Shock Wave

John C. Raymond,[1]

Richard J. Edgar,[1]

Parviz Ghavamian[2]

and

William P. Blair[3]

Received _____; accepted _____

[1]Harvard-Smithsonian Center for Astrophysics, 60 Garden St., Cambridge, MA 02138, USA; jraymond@cfa.harvard.edu

[2]Dept. of Physics, Astronomy & Geosciences, Towson University, Towson, MD 21252

[3]Department of Physics and Astronomy, Johns Hopkins University, 3400 N. Charles St., Baltimore, MD 21218, USA

ABSTRACT

Observations of SN1006 have shown that ions and electrons in the plasma behind fast supernova remnant shock waves are far from equilibrium, with the electron temperature much lower than the proton temperature and ion temperatures approximately proportional to ion mass. In the $\sim$360 km s^{-1} shock waves of the Cygnus Loop, on the other hand, electron and ion temperatures are roughly equal, and there is evidence that the oxygen kinetic temperature is not far from the proton temperature. In this paper we report observations of the He II λ1640 line and the C IV λ1550 doublet in a 360 km s^{-1} shock in the Cygnus Loop. While the best fit kinetic temperatures are somewhat higher than the proton temperature, the temperatures of He and C are consistent with the proton temperature and the upper limits are 0.5 and 0.3 times the mass-proportional temperatures, implying efficient thermal equilibration in this collisionless shock. The equilibration of helium and hydrogen affects the conversion between proton temperatures determined from Hα line profiles and shock speeds, and that the efficient equilibration found here reduces the shock speed estimates and the distance estimate to the Cygnus Loop of Medina et al. (2014) to about 800 pc.

Subject headings: shock waves; ISM: supernova remnants; dust; ISM: individual (Cygnus Loop); ultraviolet: ISM instruments: HST(COS)

1. Introduction

It is often assumed that astrophysical shock waves produce Maxwellian velocity distributions in the downstream plasma and that all particle species have the same temperature. However, in the modest number of cases where temperatures of different species can be measured, this is usually not the case. Shock waves in settings such as the solar wind, the interstellar medium, and galaxy clusters are collisionless, in that the shock transition occurs on a scale comparable to the proton gyroradius, which is orders of magnitude smaller than the collisonal mean free path. In this case, one might expect that a collisionless shock thermalizes a fraction of the kinetic energy of each incoming particle, leading to mass-proportional temperatures. The actual situation is more complex.

Typical shock waves in the solar wind have modest Mach numbers, and they generally produce electron temperatures T_e around 0.2 times the proton temperatures T_p, while heavier ions are preferentially heated, $T_i > T_p$ (Ghavamian et al. 2013; Korreck et al. 2007). In the higher Mach number shocks in supernova remnants (SNRs), T_e/T_p declines from about 1 to less than 0.1 as the shock speed increases from about 350 km s^{-1} to 2000 km s^{-1} (Ghavamian et al. 2001, 2002; Hughes et al. 2000; Ghavamian et al. 2007a; van Adelsberg et al. 2008; Medina et al. 2014). Ion temperatures in SNR shocks have been more difficult to measure, but $T_i \simeq m_i T_p/m_p$ for helium, carbon and oxygen in a 2000-3000 km s^{-1} shock in SN1006 (Raymond et al. 1995; Laming et al. 1996; Korreck et al. 2004; Broersen et al. 2013), while the oxygen temperature is less than 1.7 times the proton temperature in a 350 km s^{-1} shock in the Cygnus Loop (Raymond et al. 2003). However, coulomb collisions affect the oxygen temperature in the Cygnus Loop. In the $\simeq$ 900 km s^{-1} shocks in the LMC supernova remnant DEM L71, the kinetic temperature of O derived from the O VI line widths is about 6.5 times the proton temperature, though this is somewhat uncertain due to interstellar absorption and the contribution of bulk motions to the line

width (Ghavamian et al. 2007b). The shocks in galaxy clusters are as fast as the shocks in young SNRs, but the pre-shock temperatures are so high that the Mach number is only around 3. Some seem to show rapid electron-ion temperature equilibration, while others do not (Russell et al. 2012).

Direct measurements of velocities in solar wind shocks generally show non-Maxwellian distributions (Thomsen et al. 1990). Particle distributions in SNR shocks are non-Maxwellian in the sense that they have power-law tails of relativistic particles, but little is known about the velocity distribution of the vast majority of particles in the core of the velocity distribution. There is some evidence for a non-thermal distribution at one position in Tycho's SNR, but it is ambiguous (Raymond et al. 2010). Simulations with particle-in-cell codes tend to show Maxwellian cores with power-law tails (Caprioli et al. 2014).

In this paper we measure the kinetic temperatures of helium and carbon from profiles of the UV lines of He II and C IV obtained with the COS spectrograph on the Hubble Space Telescope. We observed a 360 km s^{-1} shock in the Cygnus Loop for which electron-ion temperature ratio is close to 1 (Medina et al. 2014). In order to interpret the observations we needed the line profile of the COS instrument with the G160M grating for an extended source, so we observed a position in the planetary nebula NGC 6853. We also compute the effects of optical depth and Coulomb collisions on the line profiles. We find that the helium and carbon kinetic temperatures, like the electron temperature, are close to the proton temperature.

2. Observations and Data Reduction

The target position in the Cygnus Loop coincides with the single orbit COS spectrum labeled Pos 1 in Raymond et al. (2013) and the Hα observation labeled COS1 in Medina et al. (2014). Nine more orbits were obtained with COS using the G160M grating set at 1577 Å; 4 orbits on 2014 October 3 and 5 orbits on 2014 November 11. They were combined with the earlier exposure for a total observation time of 29,100 seconds. The circular entrance aperture is 2.5″ in diameter.

The position is shown in Figure 1, which also shows the two positions behind the shock reported in Raymond et al. (2013). It was chosen to be slightly behind the brightest Hα emission based on the ionization times required to reach He II and C IV in the shocked gas. The coordinates are RA(2000) = 20^h 54^m 43.611^s, Dec(2000) = +32° 16′ 3.53″. For comparison, we include and X-ray image from *Chandra* and and NUV image from *Galex*. The X-rays show that the shock coincides with the jump in electron temperature. The structure in the *Galex* image is very similar to that seen in Hα. This is probably because the *Galex* NUV passband from about 1900 Å to 2750 Å is dominated by the 2-photon continuum of hydrogen in the this non-radiative shock, and that continuum from the 2s level of H is excited in a manner similar to the n=3 levels that produce Hα.

The orientation of the dispersion axis of the COS instrument was close to the long direction of the filament for the longer observations (18° and 16° away), though it was nearly perpendicular to the filament (70°) for the earlier single orbit exposure. Because the dispersion direction was along the filament for 90% of the exposure time, we assume that the emission filled the aperture uniformly in the dispersion direction.

The position was chosen because the fluxes were known from the single orbit spectrum in Raymond et al. (2013) and because the Hα profile of Medina et al. (2014) provides the proton temperature. It also provides an electron-proton temperature ratio of >0.8,

consistent with the determination of Ghavamian et al. (2001) for a nearby position. In addition, the proper motions of the shocks in that region have been measured and the electron temperature is available from X-ray spectra (Salvesen et al. 2009; Katsuda et al. 2008). IR images from Spitzer and UV spectra from COS have been used to investigate the destruction of dust and the sputtering of carbon atoms from grains behind this shock (Sankrit et al. 2010; Raymond et al. 2013). Moreover, a FUSE spectrum of a position about 2.7′ to the NW along the same filament provides the oxygen kinetic temperature from the O VI line profile (Raymond et al. 2003).

The expected line width is comparable to the instrumental profile of COS for an extended source with the G160M grating, but no instrumental profile was available for extended sources other than the statement by France et al. (2009) that the spectral resolution is about 200 km s^{-1}. The profile is not expected to be strictly Gaussian, but to be affected by the shape of the entrance aperture. To obtain the instrument profile for an extended source of narrow emission lines through the COS aperture, we observed a position in the planetary nebula NCG 6853 (The Dumbbell) 28″ S and 2″ E of the central star. Barker (1984) reported emission line fluxes from an IUE spectrum at that position, and Goudis et al. (1978) show [O III] line profiles of NGC6853. The two positions closest to the COS position have line widths (FWHM) of about 30 and 60 km s^{-1}. An archival STIS spectrum of the central star of NGC 6853 shows saturated absorption against the stellar continuum in the C IV lines between 0 and -40 km s^{-1}, which probably removes the blue wings of the emission lines, so the width is about 30 km s^{-1}, which is small compared to the COS instrumental FWHM. At worst, the FWHM of the emission lines could be about 40 km s^{-1}, which would mean that we overestimate the width of the instrumental profile by 4%. We find that the profiles of the C IV λ1550 doublet and the He II λ1640 line in NGC 6853 can be fit with pairs of Gaussians. For the C IV lines, the FWHM is 0.40 Å and the separation is 0.86 Å, while for the He II line the best fit is FWHM = 0.47 Å and separation

= 0.93 Å. The larger width of the He II line is at least partly due to the fact that He II λ1640 is an unresolved multiplet with components spread over about 0.16 Å.

Figure 2 shows the observed line profiles along with the instrument profiles from the planetary nebula measurements described above. The Cygnus Loop profiles are somewhat wider than the instrument profile, but not by much. We fit the profiles with Gaussians convolved with the instrument profiles described above. Figure 3 displays these fits, and Table 1 shows the results with 1-σ errors, along with the corresponding kinetic temperatures. The proton and O VI temperatures from Medina et al. (2014) and Raymond et al. (2003) are included for comparison. Note that the proton temperature is not obtained directly from the Hα line width. Charge transfer between protons and neutral atoms produces a population of neutrals given by the proton thermal distribution convolved with the charge transfer cross section times the relative velocity (Chevalier & Raymond 1978), so the population of fast neutrals is similar to, but not the same as, the proton velocity distribution. We use the model of Chevalier et al. (1980) to derive the proton temperature.

3. Analysis

Table 1 shows that the kinetic temperatures of helium and carbon are indistinguishable from the proton temperature, with upper limits of 1.4 and 2.9 times the proton temperature, or 0.35 and 0.24 times the mass-proportional temperatures, respectively. Here we discuss corrections for optical depth and Coulomb scattering used to obtain those limits.

3.1. Optical depth effects

The optical filaments of the Cygnus Loop and other SNRs are tangencies of the line of sight to a thin, rippled sheet of emitting plasma (Hester 1987). Thus they are

essentially thin slabs of emission seen edge-on. Resonance lines such as the C IV doublet can have substantial optical depths along the line of sight, but small optical depths in the perpendicular direction, so that photons are scattered out of the line of sight (Long et al. 1992; Cornett et al. 1992). The net effect for lines of sight near tangency is to reduce the intensity and, because the optical depth is highest at line center, to broaden the profile (Raymond et al. 2003).

The ratios of the intrinsic emissivities and of the scattering cross sections for the C IV doublet are both 2:1, but the observed intensity ratio is 1.65:1. In the single scattering limit, the intensity at any wavelength is proportional to (1-$e^{-\tau}$), and the observed intensity ratio corresponds to optical depths at line center of about 0.65 and 0.33 for λ1548 and λ1550, respectively. Those optical depths imply increases of the FWHM by 12% and 5.3%, respectively. We correct the carbon kinetic temperatures for these broadenings in Table 1. We note that the λ1548 line is nominally wider than the λ1550 line, though the difference is easily within the uncertainties. If the apparent larger width of λ1548 were attributed to scattering, the observed relative intensities would be close to 1:1. The optical depth correction for the width of the O VI line is more severe because of its larger optical depth, and we use the value given by Raymond et al. (2003).

The He II λ1640 line is optically thin, and it is not directly affected. However, some He II λ256 photons are absorbed and 12% of the absorbed λ256 photons are converted into λ1640 photons. Since the optical depth is largest near line center, more absorptions occur close to line center, producing excess λ1640 photons near line center and making the line narrower. However, the λ256 optical depth perpendicular to the shock is about 6, and much larger along the line of sight. Therefore, He II Lyβ photons are converted to λ1640 photons over much of the line profile, and we will ignore this effect on the line width.

3.2. Coulomb Equilibration

We are interested in the ion kinetic temperatures just behind the shock front, but it takes some time for carbon to be ionized to C IV, and both He II and C IV emit over a range of distances behind the shock determined by the ionization times. During those times, Coulomb collisions will bring the kinetic temperatures toward equilibrium with the proton temperature. Thus we must compute the changes in the ion temperatures due to Coulomb equilibration to see how accurately the observed kinetic temperatures reflect the values at the shock. Both because the ionization rates are smaller for higher ionization states and because the Coulomb collision rate scales as Z^2, we expect that this equilibration will be negligible for He II, larger for C IV and quite significant for O VI.

We compute the time-dependent ionization states of He, C and O using the electron temperature from X-rays of $2{\times}10^6$ K with the ionization rates of Dere (2007) as compiled in version 7 of CHIANTI (Landi et al. 2012). We use a proton temperature of 1.8×10^6 K from the Hα profile with ion-proton equilibration rates from Spitzer (1956). The difference between the two assumed temperatures lies within the uncertainties. As a limiting case, we assume mass-proportional initial temperatures, $T_{He} = 7.2 \times 10^6$ K, $T_C = 2.2 \times 10^7$ K and $T_O = 2.9 \times 10^7$ K, with all the ions starting in the singly ionized state. The density does not matter, because the ionization and Coulomb collision rates scale in the same way with n_e.

The top panel of Figure 4 shows the kinetic temperatures of He II, C IV and O VI ions as functions of time for a density of 2.0 cm^{-3}. It is apparent that carbon and oxygen approach equilibrium relatively quickly because of the Z^2 dependence of the Coulomb collision rates. This plot is not very useful, however, because nearly all of the oxygen is in lower ionization states at short times and in higher ones at long times. The middle panel shows the ionization fractions of He II, C IV and O VI as functions of the kinetic temperatures of those ions. The result, as expected, is that the average kinetic

temperature of the He II is the same as the initial temperature. The carbon ionization fraction peaks when the C IV kinetic temperature had dropped noticeably, and the O VI kinetic temperature has dropped even more sharply before the peak ionization fraction has been reached.

The bottom panel in Figure 4 shows the fractional contribution to the emission for each ion as a function of temperature in 10^6 K bins. The emission of He II is confined to a single bin, while the emission of C IV is concentrated between 1.6×10^7 and 2.1×10^7 K, with a tail at lower temperatures. The O VI emission peaks in the bin between 2×10^6 and 3×10^6 K with a long tail at higher temperatures. The peak of the O VI contribution in the low temperature bin close to the proton temperature comes about because the oxygen spends a lot of time at those kinetic temperatures, which compensates for the modest ionization fraction. The average temperatures are 7.2×10^6, 1.7×10^7 and 5.6×10^6 K for He II, C IV and O VI, respectively, or 1.0, 0.77 and 0.2 times the mass-proportional temperatures. We computed similar models for a range of intial temperatures and find that the upper limits in Table 1 are compatible with intial temperatures of 0.5, 0.3 and 0.5 times the mass proportional temperatures for He, C and O, respectively. Smaller values would be needed to match the best fit temperatures.

The fact that C IV and O VI are formed over a range of temperature means that their line profiles are the sum of Maxwellians, so they will deviate from Gaussians. The C IV line is formed over a range of about 25% in temperature or 13% in thermal speed, so detecting the departure from Maxwellian would require better data than the spectrum presented here. The O VI profile from a shock with mass-proportional heating would give a core with a temperature just above the proton temperature plus broad wings containing a large part of the flux. While the some of the profiles shown in Raymond et al. (2003) show a hint of a wing on the red side, there is no indication of the strong wings predicted by a model with

mass-proportional temperatures.

Thus we can ignore Coulomb collisions for the He II line, and the C IV lines widths are affected at the 12% level, but the O VI profiles presented by Raymond et al. (2003) are severely affected. In the faster shocks in DEM L71 (Ghavamian et al. 2007b) and SN1006 (Raymond et al. 1995; Korreck et al. 2004), the higher electron and ion temperatures greatly reduce the ionization time scales and increase the Coulomb collision time scale, so that Coulomb collisions can be neglected even for O VI.

3.3. Interpretation

First we discuss the kinetic temperatures that might be expected in a collisionless shock. To first order, such a shock simply thermalizes 3/4 of the shock speed independently for each species, leading to mass-proportional ion temperatures, approximately as seen in the 3000 km s^{-1}shock in SN1006 (Raymond et al. 1995; Korreck et al. 2004).

The situation is more complicated for species that enter the shock as neutral atoms or in dust grains. Much of the helium is neutral, and about 75% of the carbon is in the form of PAHs or dust (Raymond et al. 2013). The PAHs dissociate very quickly behind the shock and contribute to the observed line profile (Micelotta et al. 2010), while dust grains sputter away more gradually over tens of arcseconds at the distance of the Cygnus Loop (Raymond et al. 2013) and do not contribute much to the profile at the shock. Neutrals that pass through the shock and become ionized downstream are expected to behave as pickup ions (Raymond et al. 2008). For quasi-perpendicular shocks, the velocity component along the field is conserved while the component perpendicular to the field forms a ring beam in velocity space. The unstable ring distribution quickly scatters into a hollow bispherical shell in velocity space by emitting and absorbing Alfvén waves (Williams & Zank 1994;

Isenberg 1995). The distribution then scatters into a Maxwellian, though the temperatures parallel and perpendicular to the field may differ. If the distribution is too anisotropic, either firehose or mirror instabilities will drive the anisotropy toward marginal instability (Maruca et al. 2012). Such a pickup ion process in the partially neutral hydrogen provides one of several possible interpretations for the non-Maxwellian Hα profile observed at knot "g" in Tycho's supernova remnant (Raymond et al. 2010), and it is responsible for the motion of oxygen ions along field lines seen in images of the sungrazing comet C/2011 W3 (Lovejoy) (Raymond et al. 2014). The poor fit of the He II profile to a Gaussian velocity distribution, $\chi^2 = 2.4$, might suggest a pickup ion contribution added to a Maxwellian, but the data do not warrant a strong conclusion. We note that the sharp peak to the right of the centroid is much narrower than the instrumental resolution and must therefore be a result of the modest number of counts in the line.

The comet observations also confirm that a significant fraction of the energy in the ring distribution can be lost to waves, depending on the Alfvén speed and angle between the flow and the magnetic field (Williams & Zank 1994). For the shock observed here, the post-shock Alfvén speed is around 20-30 km s^{-1}, and the loss to waves should be small (Raymond et al. 2008). The final temperature of the pickup ions depends on the angle between the field and the shock, and for quasi-perpendicular shocks it will be between 0.5 and 1 times the mass-proportional temperature.

Many of the C and O atoms are already ionized when they pass through the shock. Because of their high mass to charge ratios, these ions are not slowed as much by the electrostatic field in the shock wave as are the protons. According to Fuselier & Schmidt (1997) they will be about 25% hotter than the protons. Lee & Wu (2000) and Zimbardo (2011) also present models for strong preferential heating of heavy ions in shocks. Those models predict very high ratios of perpendicular to parallel temperatures, $T_\perp/T_\parallel$. Depending

upon the angle between the magnetic field and our line of sight, we could in principle observe mainly $T_\parallel$ and therefore a low temperature. However, large $T_\perp/T_\parallel$ would generate mirror mode instabilities and, for the high plasma β in this shock, sharply reduce the anisotropy (Maruca et al. 2012). Solar wind observations of modest Mach number shocks show some preferential heating of heavy ions, but there is little correlation with shock parameters (Korreck et al. 2007).

There is also transfer of energy among species by plasma waves and turbulence at the shock. Waves can be excited upstream of the shock jump by streaming instabilities generated either by particles reflected by the shock or by cosmic rays (Thomsen et al. 1990; Laming et al. 2014). For example, Ghavamian et al. (2007a) and Rakowski et al. (2008) show that lower hybrid waves in a cosmic ray precursor can heat the electrons to $T_e \simeq T_p$ in shocks at about the speed of the one observed here.

Our observations give upper limits to He and C temperatures of 1.4 and 2.9 times the proton temperature found by Medina et al. (2014). After considering Coulomb collisions, the upper limits on the initial temperatures are 2 and 4 times the proton temperature, and the O VI profile of Raymond et al. (2003) gives an upper limit of 8 times the proton temperature. This contrasts with the nearly mass proportional values (4, 12 and 16) seen in the 2000-3000 km s^{-1}shock in SN1006 (Raymond et al. 1995; Korreck et al. 2004), and it is similar to the indications of nearly complete electron-ion equilibration in the Cygnus Loop compared with $T_e/T_i \simeq 0.05$ in SN1006 (Ghavamian et al. 2002; van Adelsberg et al. 2008). It indicates rapid temperature equilibration by plasma waves and turbulence in the Mach 35 Cygnus Loop shock, while the equilibration in the Mach 200-300 SN1006 shock is ineffective.

The effective equilibration of the particle species has an important implication for the derivation of shock speeds from Hα line widths. As shown by Chevalier et al. (1980) and

van Adelsberg et al. (2008), if the energy dissipated in the shock is shared among electrons and ions, a higher shock speed is needed to account for a given line width. On the other hand, if helium is efficiently equilibrated, the proton temperature behind a shock of a given speed is increased. Medina et al. (2014) assumed that helium remained mostly neutral through the region where the Hα line is formed and that the T_e and T_i are equal, so that the post-shock temperature is given by 1/2 the thermalized proton speed. On the other hand, we find that helium is brought to close to the ion temperature close to the shock, in which case the kinetic energy of the helium is shared with the protons. While Medina et al. (2014) found a shock speed of 405 km s^{-1}, a shock speed as low as $\sim$ 360 km s^{-1}could account for the Hα profile if $T_H = T_{He}$ where the Hα line forms. (We assume a helium abundance of 10% by number. If most of the helium is neutral and it is mostly ionized only after the hydrogen is ionized, the effect will be smaller.) When that lower shock speed is combined with the proper motion measured by Salvesen et al. (2009), the distance to the Cygnus Loop is reduced from 890 pc to 800 pc. That partially alleviates the disagreement between the proper motion distance and the upper limit of 640 pc to the distance from the detection of SNR absorption lines (Blair et al. 2009) in the spectrum of a background star, but it still leaves a substantial discrepancy. Of course, if a significant fraction of the shock energy goes into cosmic rays, a correspondingly higher shock speed would be required. Shimoda et al. (2015) point out that comparison of the shock speed derived from the proper motion with the shock parameters determined from the shock jump conditions can be misleading, as a shock in a realistic ISM density distribution is somewhat oblique at most positions. However, for the shock observed here, Medina et al. (2014) measured the offset between the velocity centroids of the broad and narrow Hα to be only 9 km s^{-1}, so the obliquity is very small.

4. Summary

We have measured He and C kinetic temperatures behind a moderate velocity shock in the Cygnus Loop. Unlike the fast shock in SN1006, where the temperatures are mass-proportional, in the Cygnus Loop they are nearly the same. We have shown that Coulomb equilibration is not important for the He II line, and it affects the C IV lines at the 33% level, so the equilibration must occur at the shock front by means of plasma turbulence. However, Coulomb collisions severely affect the kinetic temperature of O VI if it is initially higher than the proton temperature, so that the C IV and He II lines provide better constraints on temperatures at the shock than do the O VI lines for this relatively slow SNR shock. The rapid equilibration of helium suggests that the post-shock protons are partly heated by helium, which would reduce the shock speed required, and hence the distance inferred from proper motions, by as much as 11%. It is important that the the thermal equilibration of protons, electrons and helium be considered when converting Hα line widths of Balmer line filaments into shock speeds.

The degree of ion-ion equilibration and the related heating processes may be important for determining the efficiency of injection of the different species into the cosmic ray acceleration process. Besides that, it is potentially useful as a diagnostic for the plasma waves that produce the shock transition in a collisionless shock.

We determined the instrumental profile of the COS spectrograph for an extended source with the G160M grating by observing a planetary nebula, and this may be useful for other studies of extended sources that fill the COS aperture. The $\simeq$ 200 km s^{-1} wide instrumental profile can be described as a pair of Gaussians with FWHM = 0.40 Å separated by 0.86 Å.

The authors thank the referee for requesting an additional plot, which revealed a

numerical error in the average temperatures, and for other useful suggestions. This work was performed under grants HST-GO-12885 and HST-GO-13436 to the Smithsonian Astrophysical Observatory. RJE was supported by NASA contract NAS8-03060. JR and PG thank Lorentz Center Workshop on Particle Acceleration from the Solar System to Cosmology for useful discussions.

Facilities: HST (COS)

REFERENCES

Barker, T. 1984, ApJ, 284, 589

Blair, W.P., Sankrit, R. & Raymond, J.C. 2005, AJ, 129, 2268

Blair, W.P., Sankrit, R., Torres, S.I., Chayer, P. & Danforth, C.W. 2009, ApJ, 692, 335

Broersen, S., Vink, J., Miceli, M., Bocchino, F., Maurin, G. & Decourchelle, A. 2013, A&A, 552, 9

Caprioli, D., Pop, A.-R. & Spitkovsky, A. 2014, astro-ph 1409.8291

Chevalier, R.A., & Raymond, J.C. 1978, ApJ, 225, L27

Chevalier, R.A., Kirshner, R.P. & Raymond, J.C. 1980, ApJ, 235, 186

Cornett, R.H., et al. 1992, ApJL, 395, 9

Dere, K.P. 2007, A&A, 466, 771

Dere, K.P., Landi, E., Young, P.R., Del Zanna, G., Landini, M. & Mason, H.E. 2009, A&A, 498, 915

France, K., et al. 2009, ApJ, 707, L27

Fuselier, S.A. & Schmidt, W.K.H. 1997, JGRA, 102, 11273

Ghavamian, P., Raymond, J.C., Smith, R.C. & Hartigan, P. 2001, ApJ, 547, 995

Ghavamian, P., Winkler, P.F., Raymond, J.C. & Hartigan, P. 2002, ApJ, 572, 888

Ghavamian, P. Laming, J.M., & Rakowski, C.E. 2007a, ApJL, 654, L69

Ghavamian, P. Blair, W.P., Sankrit, R., Raymond, J.C. & Hughes, J.P. 2007b, ApJ, 664, 304

Ghavamian, P., Schwartz, S.J., Mitchell, J., Masters, A. & Laming, J.M. 2013, SSRV, 178, 633

Goudis, C., McMullan, D., Meaburn, J., Tebbutt, N.J. & Terrett, D.L. 1978, MNRAS, 182, 13

Hester, J.J. 1987, ApJ, 314, 187

Hughes, J.P., Rakowski, C.E. & Decourchelle, A. 2000, ApJL,543, L61

Isenberg, P.A. 1995, Rev. Geophys., 3, 623

Katsuda, S., Tsunemi, H., Kimura, M. & Mori, K. 2008, ApJ, 680, 1198

Korreck, K.E., Raymond, J.C., Zurbuchen, T.E. & Ghavamian, P. 2004, ApJ, 615, 280

Korreck, K.E., Zurbuchen, T.E., Lepri, S.T. & Raines, J.M. 2007, ApJ, 659, 773

Laming, J.M., Raymond, J.C., McLaughlin, B.M. & Blair, W.P. 1996, ApJ, 472, 267

Laming, J.M., Hwang, U., Ghavamian, P. & Rakowski, C. 2014, ApJ, 790, 11.

Landi, E. Del Zanna, G., Young, P.R., Dere, K.P. & Mason, H.E. 2012, ApJS, 744, 99

Lee, L.C. & Wu, B.H 2000, ApJ, 535, 1014

Long, K.S., Blair, W.P., Vancura, O., Bowers, C.W., Davidsen, A.F. & Raymond, J.C. 1992, ApJ, 200, 214

Maruca, B.A, Kasper, J.C. & Gary, S.P. 2012, ApJ, 748, 137

Medina, A., Raymond, J.C., Edgar, R.E., Caldwell, N., Fesen, R.A. & Milisavljevic, D. 2014, ApJ, 791, 30

Micelotta, E.R., Jones, A.P. & Tielens, A.G.G.M. 2010, A&A, 510, A37

Rakowski, C.E., Laming, J.M. & Ghavamian, P. 2008, ApJ, 684, 348

Raymond, J.C., Blair, W.P. & Long, K.S. 1995, ApJ, 454, L31

Raymond, J.C., Ghavamian, P., Sankrit, R., Blair, W.P. & Curiel, S. 2003, ApJ, 584, 770

Raymond, J.C., Isenberg, P.A., & Laming, J.M. 2008, ApJ, 682, 408

Raymond, J.C., Winkler, P.F., Blair, W.P., Lee, J.-J. & Park ,S. 2010, ApJ, 682, 408

Raymond, J.C., Ghavamian, P., Williams, B.J., Blair, W.P., Borkowski, K.J., Gaetz, T.J. & Sankrit, R. 2013, ApJ, 778, 161

Raymond, J.C., McCauley, P.I., Cranmer, S.R. & Downs, C. 2014, ApJ, 788, 152

Russell, H.R., et al. 2012, MNRAS, 432, 236

Salvesen, G., Raymond, J.C. & Edgar, R.E. 2009, ApJ, 702, 327

Sankrit, R., et al. 2010, ApJ, 712, 1092

Shimoda, J., Inoue, T., Ohira, Y., Yamazaki, R., Bamba, A. & Vink. J. 2015, astro-ph 1412.2874v1

Spitzer, L., 1956 *The Physics of Fully Ionized Gases*, (New York: Interscience Publication)

Thomsen, M.F., Gosling, J.T., Bame, S.J. & Onsager, T.G. 1990, JGRA, 95, 6363

van Adelsberg, M., Heng, K., McCray, R., & Raymond, J.C. 2008, ApJ, 689, 1089

Williams, L.L., & Zank, G.P. 1994, JGR, 99, 19229

Zimbardo, G. 2011, P&SS, 59, 468

This manuscript was prepared with the AAS LaTeX macros v5.2.

Table 1

Fit Parameters

Temperatures in units of 10^6 K

Line	FWHM (km s^{-1})	T_{kin} (10^6 K)	T_{corr} (10^6 K)	χ^2/DOF
H I λ6563	254^{+16a}_{-16}	$1.8^{+0.3b}_{-0.3}$		
He II λ1640	106^{+39}_{-40}	$2.0^{+1.8}_{-1.2}$	$2.0^{+1.8}_{-1.2}$	2.46
C IV λ1548	106^{+25}_{-42}	$5.9^{+3.2}_{-3.7}$	$4.7^{+2.5}_{-3.0}$	1.33
C IV λ1550	72^{+35}_{-71}	$2.7^{+3.2}_{-2.7}$	$2.4^{+2.8}_{-2.4}$	1.43
O VI λ1032	120	5.1^c	$<3.2^c$	

a Hα line width from Medina et al. (2014)

b Hydrogen temperature based on model proton temperature leading to observed line width after charge transfer (Medina et al. 2014)

c From Raymond et al. (2003). The temperature is 3.2×10^6 K after correction for optical depth effects.

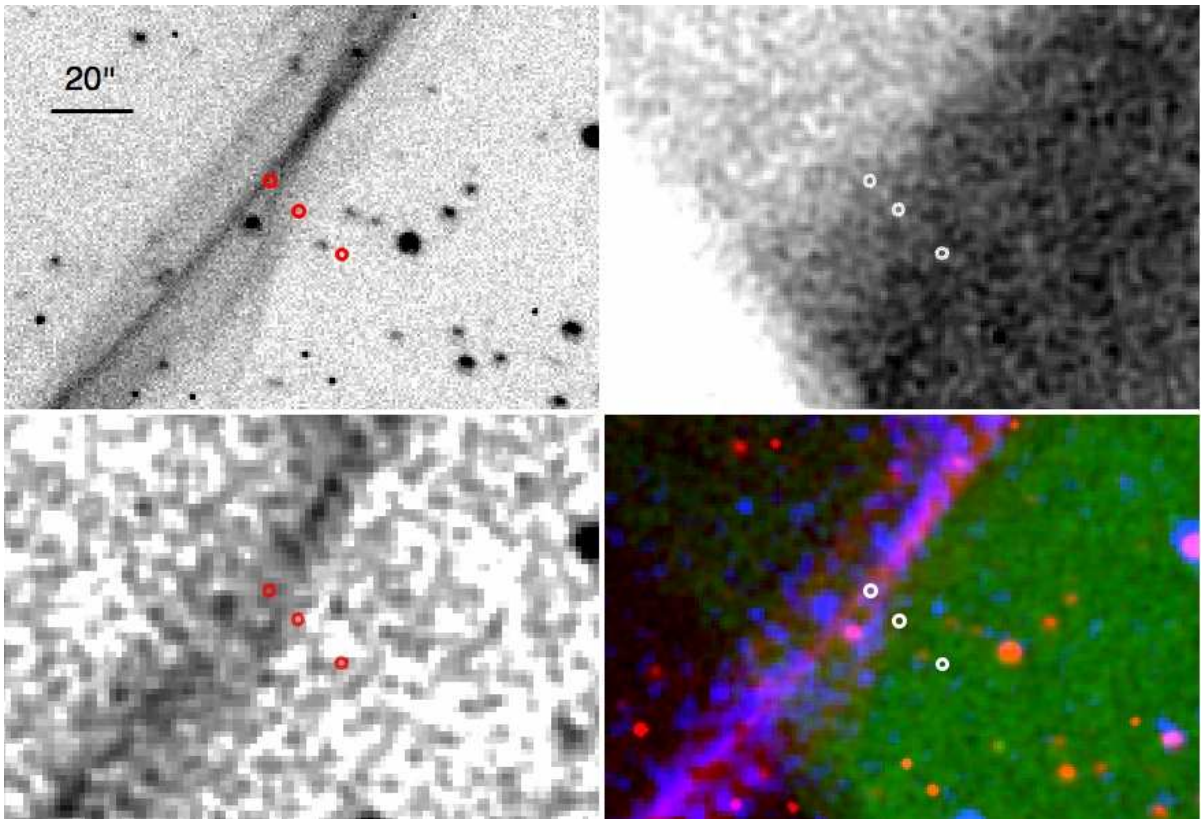

Fig. 1.— COS aperture positions of Raymond et al. (2013) overlaid on Hα, *Chandra* X-ray and Galex NUV images. The lower right hand panel shows the apertures overlaid on a 3 color superposition of Hα (red), NUV (blue) and X-rays (green). The position observed here is the one at the upper left on the Hα filament.

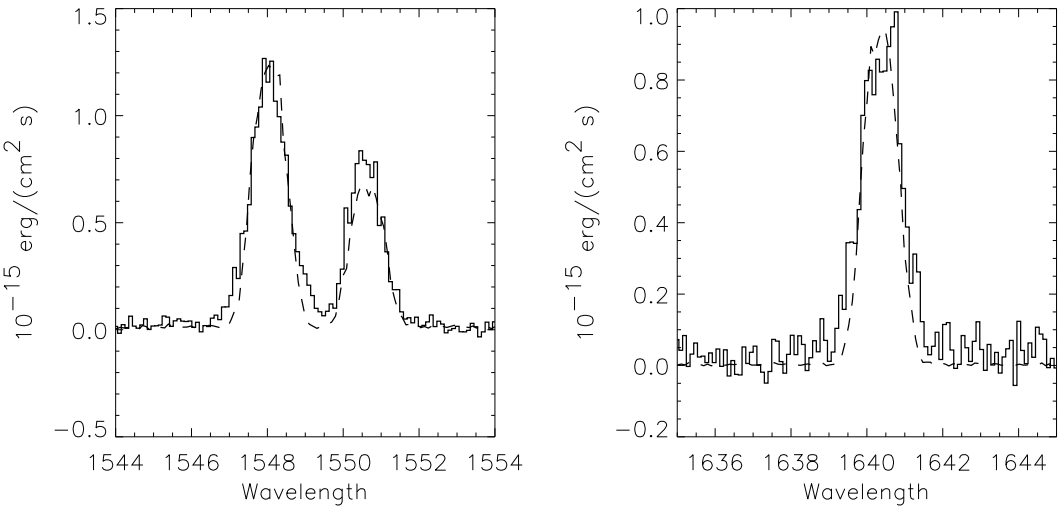

Fig. 2.— Observed C IV doublet and He II λ1640 lines from the Cygnus Loop (solid) compared with the instrument profiles derived from the spectrum of the planetary nebula NGC 6853 (dashed).

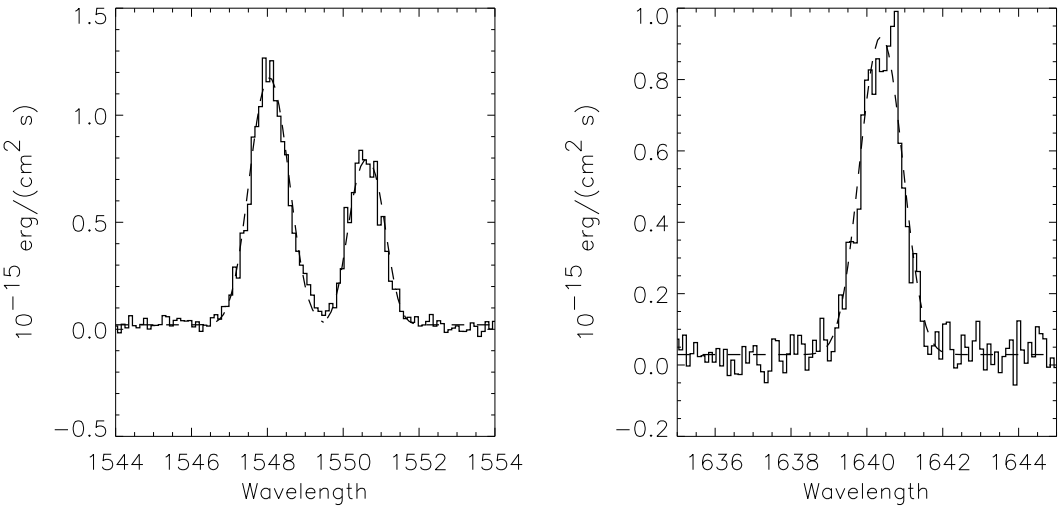

Fig. 3.— Observed C IV doublet and He II λ1640 observed profiles (solid) compared with best fit Gaussians convolved with the planetary nebula line profiles (dashed).

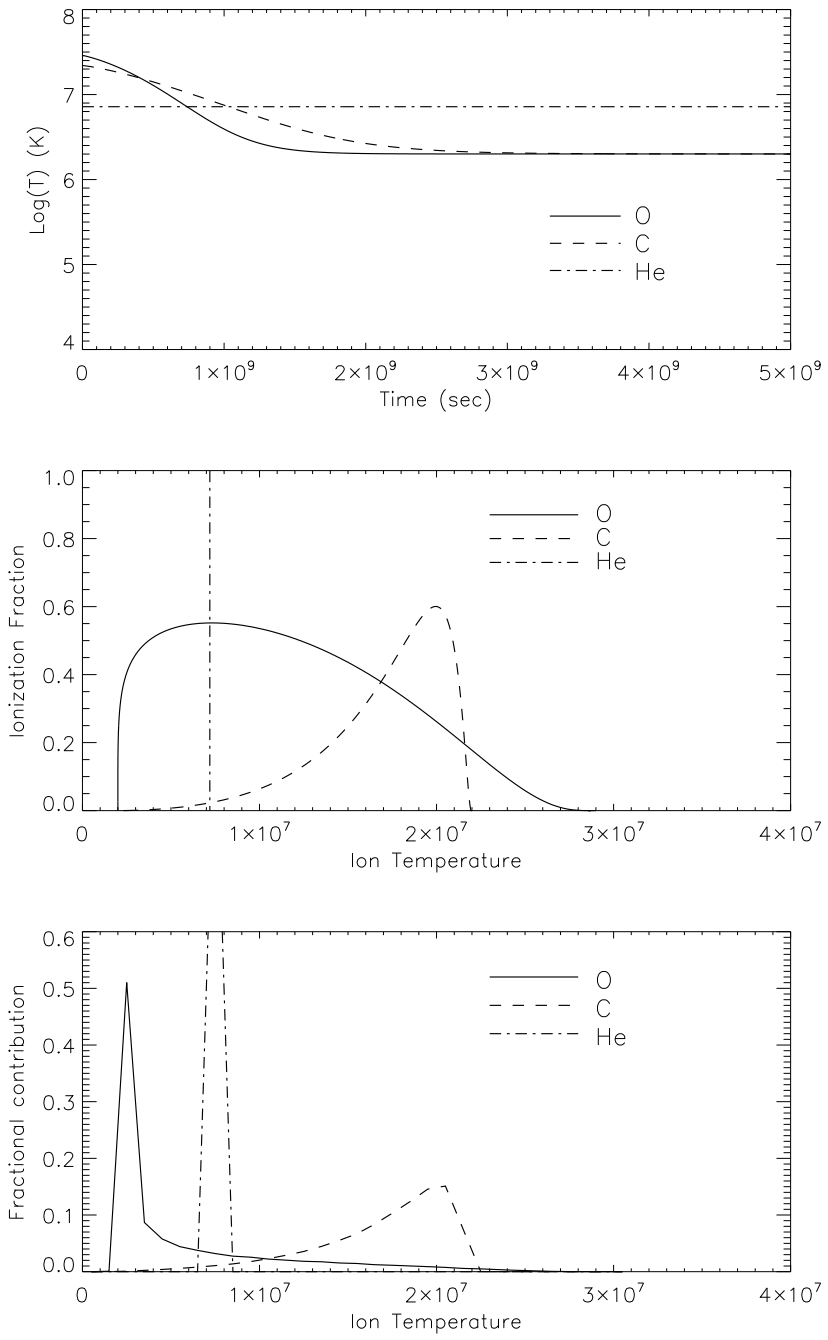

Fig. 4.— Top panel. Kinetic temperatures of He II, C IV and O VI as functions of time behind the shock front. Middle panel. Ionization fractions of He II, C IV and O VI as functions of kinetic temperature. While Coulomb collisions have no effect on helium before He II is ionized away, and only a small effect on the the temperature of carbon before C IV is ionized to C V, the temperature of oxygen is driven toward the proton temperature by the time O VI is ionized. Bottom panel. Contribution fractions to the emission of each line